CHIN. PHYS. LETT. Vol. 38, No. 8 (2021) 087102

Coexistence of Charge Order and Antiferromagnetic Order in an Extended Periodic Anderson Model

Yanting Li(李艳婷), Bixia Gao(高碧霞), Qiyu Wang(王启宇), Juan Zhang(张娟), and Qiaoni Chen(陈巧妮)*

Department of Physics, Beijing Normal University, Beijing 100875, China

(Received 2 June 2021; accepted 12 July 2021; published online 2 August 2021)

The competition between the RKKY interaction and the Kondo effect leads to a magnetic phase transition, which occurs ubiquitously in heavy fermion materials. However, there are more and more experimental evidences indicating that the valence fluctuation plays an essential role in the Ce- and Y-based compounds. We study an extended periodic Anderson model (EPAM) which includes the onsite Coulomb repulsion U_{cf} between the localized electrons and conduction electrons. By employing the density matrix embedding theory, we investigate the EPAM in the symmetric case at half filling. By fixing the onsite Coulomb repulsion U of the localized electrons to an intermediate value, the interplay between the RKKY interaction, the Kondo effect and the Coulomb repulsion U_{cf} brings rich physics. We find three different phases, the antiferromagnetic phase, the charge order phase and paramagnetic phase. When the hybridization strength V between the localized orbital and the conduction orbital is small, the Kondo effect is weak so that the AF phase and the CO phase are present. The phase transition between the two long-range ordered phase is of first order. We also find a coexistence region between the two phases. As V increases, the Kondo effect becomes stronger, and the paramagnetic phase appears between the other two phases.

DOI: 10.1088/0256-307X/38/8/087102

Valence fluctuation phenomena occur in rare-earth compounds.[1] The proximity of the $4f$ level to the Fermi energy leads to instabilities of the charge configuration. The study of valence fluctuation phenomena is important in three different aspects. First, there are more and more experiments recently in the Yb-based compounds and the Ce-based compounds, indicating that valence fluctuation plays an import role in the unconventional quantum critical behaviors.[2,3] These compounds include β-$YbAlB_4$,[4,5] $YbRh_2Si_2$,[6] $YbInCu_4$,[7] $YbRh_2(Si_{0.95}Ge_{0.05})_2$,[8] $YbAuCu_4$,[9], and $Ce_{0.9-x}La_xTh_{0.1}$.[10] Second, it is believed that there exists another origin of unconventional superconductivity besides spin fluctuation. Such as the second superconducting phase in $CeCuSi_2$ and $CeCuGe_2$ under high pressure.[11−13] Third, it was suggested to induce Lifshitz transition in $CeAl_3$.[14] Besides the above aspects, valence fluctuation plays an important role in the mixed valence compound $EuNi_2P_2$,[15] and also in the hybridization wave in URu_2Si_2.[16]

The periodic Anderson model (PAM) is the minimal model which captures the physics of heavy fermions. It includes both the charge and spin degrees of freedom. However it is unable to describe valence fluctuation. The extended periodic Anderson model (EPAM) includes Coulomb repulsion between the intra-site conduction and localized orbitals. Therefore, the charge interactions becomes more significant compared with the standard PAM. Meanwhile, the valence fluctuation plays a more important role, and more exotic charge ordered phase would appear. It was suggested that the correlation between the conduction electrons and localized electrons stabilize the valence transition.[17,18] The exotic quantum critical phenomena in several Yb-based compounds and Ce-based compounds are connected with the sharp valence transition or valence crossover. The EPAM has been studied intensively before, e.g., the study of the three-dimensional model by slave boson large-N expansion,[19] the study of EPAM on a Bethe lattice by dynamical mean field theory (DMFT),[20,21] the study of EPAM on the Penrose lattice by DMFT,[22] the study of one-dimensional EPAM by density matrix renormalization group (DMRG),[17,23,24] as well as the study of one-dimensional EPAM by projector-based renormalization approach.[25]

In this Letter, we study the EPAM on a honeycomb lattice by density matrix embedding theory (DMET).[26] First, we briefly describe the model and provide details of the method. Then, our main results on the phase diagrams, physical quantities and discussions are given. Finally, a summary is provided.

We study an extended periodic Anderson model (EPAM) which includes Coulomb repulsion between

Supported by the National Natural Science Foundation of China (Grant Nos. 11974048 and 11974049), and the Beijing Science Foundation (Grant No. 1192011).

*Corresponding author. Email: qiaoni@bnu.edu.cn

© 2021 Chinese Physical Society and IOP Publishing Ltd

intra-site c–f orbitals. The Hamiltonian is

$$H = -t\sum_{\langle ij\rangle\sigma}(c^{\dagger}_{i\sigma}c_{j\sigma}+\text{H.c.}) + V\sum_{i\sigma}(c^{\dagger}_{i\sigma}f_{i\sigma}+\text{H.c.}) + E_f\sum_{i\sigma}f^{\dagger}_{i\sigma}f_{i\sigma} + U\sum_i n^f_{i\uparrow}n^f_{i\downarrow} + U_{cf}\sum_i n^f_i n^c_i, \quad (1)$$

where $c_{i\sigma}$ ($f_{i\sigma}$) is the annihilation operator of conduction (localized) orbitals at site i in spin states $\sigma =\uparrow,\downarrow$. The conduction orbitals c are itinerant, and the hopping integral between neighboring c orbitals is t. E_f is the onsite energy of the localized orbitals f. The hybridization strength between intrasite c and f orbitals is represented by V. In the EPAM the intersite Coulomb interactions are ignored, so only intrasite Coulomb interactions are present. The Coulomb repulsion between f orbitals are denoted by U, while between c and f orbitals are denoted by U_{cf}. Here $n^f_{i\sigma}$ is the number of electrons of f orbitals on site i with spin state σ, and $n^f_i = n^f_{i\uparrow}+n^f_{i\downarrow}$. The number of electrons of c orbitals on site i is n^c_i.

Density matrix embedding theory (DMET) was proposed in 2012.[26] It has been applied to the periodic Anderson model.[27,28] In a DMET calculation, a lattice model is mapping to an impurity model. The impurity model only includes a few sites, thus the computational cost is much more reduced. However, at the same time the computational precision still maintains.

In a DMET calculation the first step is to divide the lattice into different clusters which tile the whole lattice. Usually the clusters is chosen as one or multiple unit-cells of the lattice to keep the translation invariance. Then an auxiliary Hamiltonian h is introduced:

$$h = h_0 + v, \quad (2)$$

where h_0 is the one-body term of H, and v is the correlation potential. The correlation potential v is introduced to represent the effect of interactions. It only includes intra-cluster potential, thus v is block diagonal.

The next step is to diagonalize h, and the ground state $|\phi\rangle$ of h is derived. One of the cluster is chosen as the impurities, and the rest lattice sites are treated as environmental sites. There exist more than one transformations, by applying which to the environment orbitals, they become core orbitals, bath orbitals and virtual orbitals. The core orbitals are fully occupied, the virtual orbitals are completely empty, and the bath orbitals are entangled with the impurity orbitals. Since the core orbitals and the virtual orbitals are either occupied or empty, these degree of freedom is frozen. The impurity orbitals and the bath orbitals span an active space. The projection operator from the entire Hilbert space to the active space is P. Applying P to the auxiliary Hamiltonian h, removing the correlation potentials on the impurity sites, and bringing back the electron-electron interactions, we can reach an impurity model H_{imp} which is defined in the active space.

$$H_{\text{imp}} = PhP - \sum_{i,j\in imp} v_{ij}c^{\dagger}_{i\sigma}c_{j\sigma} + U\sum_{i\in imp} n^f_{i\uparrow}n^f_{i\downarrow} + U_{cf}\sum_{i\in imp} n^c_i n^f_i. \quad (3)$$

It can be proved that the bath orbitals are at most as many as the impurity orbitals. Thus H_{imp} only includes a few orbitals, it can be solved accurately. In this work we employ the density matrix renormalization group (DMRG) to solve the impurity model H_{imp}.[29] Since H_{imp} only includes a few orbitals, the computational cost and the entanglement between orbitals are quite similar to those in molecules. The DMRG employed here is more suitable for the quantum chemistry problems, and is momentum space DMRG instead of real space DMRG that is used more often in the lattice problems.

The new correlation potential is determined through the one particle reduced density matrix (1−PDM). The ground state of the impurity model H_{imp} is $|\Phi\rangle$, and the 1−PDM of $|\Phi\rangle$ is ρ^{I}. Our goal is to minimize the difference between $|\phi\rangle$ and $|\Phi\rangle$. The 1−PDM of $|\phi\rangle$ is ρ^0, then the new correlation potential is derived from

$$\min_v f(v) = \sqrt{\sum_{ij}|\rho^{\text{I}}_{ij} - (P\rho^0 P)_{ij}|^2}. \quad (4)$$

With the new correlation potential, the previous steps are repeated until the correlation potential converges. Thus a self-consistent loop is formed.

We have run the DMET calculations of EPAM on a two-dimensional honeycomb lattice. The honeycomb lattice is a bipartite lattice, it is constituted by sublattices A and B.[30] Each sublattice forms a triangular lattice. The unit cell of the honeycomb lattice includes two sites, one belongs to sublattice A, and the other belongs to sublattice B. Our calculation has been carried out on a lattice of 150×150 unit cells, and the cluster in our calculation is only one unit cell. Since increasing the cluster size does not change the results too much in this model,[28] in one unitcell there are two sites and the impurity model H_{imp} in our calculations includes four impurity orbitals and four bath orbitals. The solution of H_{imp} is the same as that of the system including 8 electrons occupying 8 sites. Because we study the phase diagram, we use DMRG as the impurity solver rather than Davidson to reduce the computational cost.

The ground-state phase diagrams are shown in Fig. 1. In our calculations the hopping integral t is

fixed to 1.0, and the onsite f orbital's Coulomb repulsion U is fixed to 4.0. The value of U is a mid value, it is large enough for the RKKY interactions and Kondo effect to take place, but not too large to diminish other interactions. We fix the filling at half filling ($n = n^c + n^f = 2.0$, where $n^f = \sum_i \langle n_i^f \rangle / N$, $n^c = \sum_i \langle n_i^c \rangle / N$ and N is the number of lattice sites), and we focus on the symmetric case when $E_f = -U/2$. Thus $n^c = 1.0$ and $n^f = 1.0$ is guaranteed. We find three different phases, i.e., the charge order phase (CO), the antiferromagnetic phase (AF) and the paramagnetic phase. When the interorbital Coulomb repulsion U_{cf} dominates, electrons on the same site favor to occupy different orbitals. The hopping term of the c orbitals, the onsite Coulomb repulsion of the f orbitals, as well as the difference of the chemical potential between c and f orbitals prohibit all the electrons to occupy c or f orbitals. Thus a long-range charge order is formed. When U_{cf} decreases the RKKY interaction dominant, the antiferromagnetic long-range order (AF) starts to present. However, the increase of the hybridization strength will strengthen the Kondo effect. The paramagnetic phase is present when V is of a large value. When V is of a small value, there is one coexistence region of CO phase and AF phase marked as shaded area in Fig. 1.

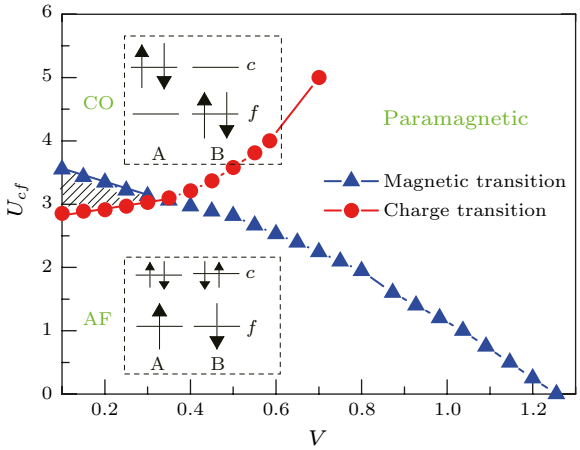

Fig. 1. Ground state phase diagram of the extended periodic Anderson model on a honeycomb lattice. There are three different phases, i.e., anti-ferromagnetic phase (AF), charge order phase (CO), and paramagnetic phase. The phase transition from the AF phase to the other phases is the magnetic phase transition, labels as blue triangles. While the phase transition from the CO phase to the other phases are charge transition, labels as red circles. The shaded area is the coexistence region where the AF phase and CO phase coexist.

The difference between the EPAM and the standard PAM is the inter-orbital Coulomb interaction U_{cf}. First, we display the effects of U_{cf}, by fixing U_{cf} to a relatively large value ($U_{cf} = 4.0$ and $U_{cf} = 5.0$), and varying V. The charge order parameter are shown by red and blue lines in Fig. 2(a), and it is defined as

$$\eta = \frac{n_{\rm A}^c - n_{\rm A}^f - n_{\rm B}^c + n_{\rm B}^f}{4}. \tag{5}$$

When the hybridization strength V is small, the inter-orbital Coulomb interaction U_{cf} dominates. The electrons prefer to occupy the same orbital in the same site. The intra-orbital Coulomb interaction U on the localized orbital f prevents the electrons from fully occupying the f orbitals. The location of the f orbital energy level E_f prevent the electrons from fully occupying the c orbitals. Thus the electrons are more likely to occupy the itinerant orbital c on some of lattice sites, and to occupy the localized orbital f on the other lattice sites. The honeycomb lattice is bipartite, so it is natural that the electrons occupy the c orbitals on sublattice A (B), and occupy the f orbitals sublattice B (A). We calculate the double occupancy of f orbitals $d_f = \langle n_\uparrow^f n_\downarrow^f \rangle$ on both sublattices A and B, and they are displayed in Fig. 2(b). When the hybridization strength V is close to 0, $d_{\rm A}^f$ is almost 0 and $d_{\rm B}^f$ is almost 1.0. The double occupancy of the c orbitals is opposite, i.e., $d_{\rm A}^c$ is almost 1.0 and $d_{\rm B}^c$ is almost 0.

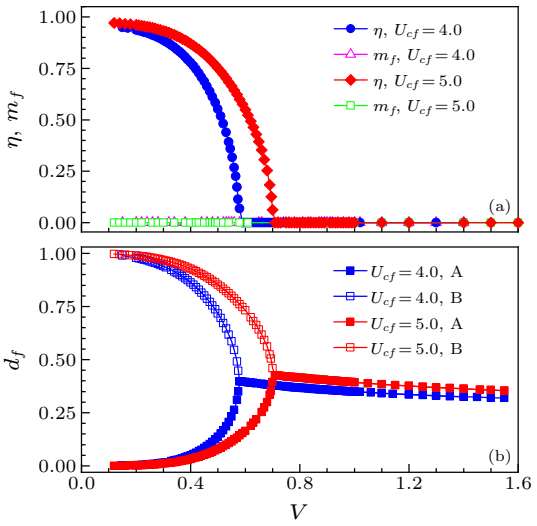

Fig. 2. Physical quantities as functions of V when $U_{cf} = 4.0$ and $U_{cf} = 5.0$. (a) Charge order parameter η and staggered magnetization m_f. The definition of charge order parameter is in Eq. (5). Blue (red) line is η when $U_{cf} = 4.0$ ($U_{cf} = 5.0$), while purple (green) line is m_f when $U_{cf} = 4.0$ ($U_{cf} = 5.0$). (b) Double occupancies of the localized f orbitals. Blue hollow (solid) squares are $d_{\rm A}^f$ ($d_{\rm B}^f$) when $U_{cf} = 4.0$, and red hollow (solid) squares are $d_{\rm A}^f$ ($d_{\rm B}^f$) when $U_{cf} = 5.0$.

As displayed in Fig. 2, as V increases the Kondo coupling J increases, and it competes with the inter-orbital Coulomb repulsion U_{cf}. The charge order becomes weaker and weaker as V increases, and disappears at certain value of V. At that time, the charge order parameter η becomes zero, and $d_{\rm A}^f = d_{\rm B}^f$. When

$U_{cf} = 4.0$ the critical hybridization $V_c = 0.59$, and when $U_{cf} = 5.0$ the critical hybridization $V_c = 0.71$. If the inter-orbital Coulomb interaction U_{cf} is larger, it requires larger value of V to kill the charge order. Besides the double occupancy and charge order parameters, we also calculate the staggered magnetization m_f of the localized f orbitals. The definition is

$$m_f = \frac{n^f_{\mathrm{A}\uparrow} - n^f_{\mathrm{A}\downarrow} - n^f_{\mathrm{B}\uparrow} + n^f_{\mathrm{B}\downarrow}}{2}. \tag{6}$$

Due to the RKKY interactions, anti-ferromagnetic long-range order is present when U_{cf} is not present, and the staggered magnetization m_f is not zero. However, the inter-orbital Coulomb repulsion U_{cf} competes with the RKKY interaction and decimates the anti-ferromagnetic long-range order. When $U_{cf} = 4.0$ and $U_{cf} = 5.0$, m_f is always zero no matter how V changes.

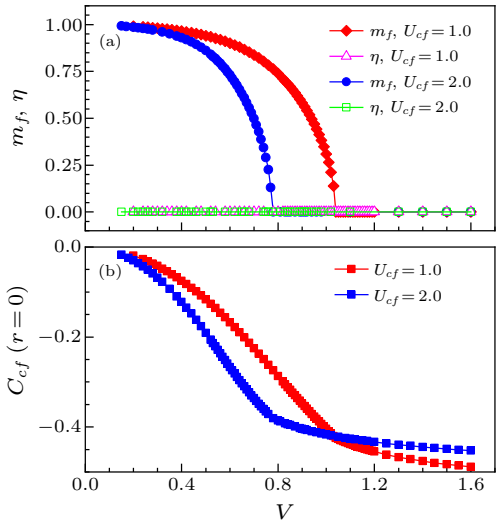

Fig. 3. Physical quantities as functions of V when $U_{cf} = 1.0$ and $U_{cf} = 2.0$. (a) Staggered magnetization of localized f orbital m_f. The red line red line is when $U_{cf} = 1.0$, and the blue line is when $U_{cf} = 2.0$. The purple and green lines are for the charge order parameter η when $U_{cf} = 1.0$ and $U_{cf} = 2.0$. (b) Spin-spin correlation functions between c orbital and f orbital on the same site.

Next we fix $U_{cf} = 1.0$ and $U_{cf} = 2.0$ to see if the charge order still exists. We calculate the charge order parameter η and the staggered magnetization m_f. The charge order parameter η is always zero as displayed in Fig. 3(a) (the magenta and green lines). Although the charge order disappears, the anti-ferromagnetic long-range order is present. The staggered magnetization m_f decreases as V increases, since the Kondo effect plays a more and more important role. It is displayed as red and blue lines in Fig. 3(a). It is worth mentioning the behavior of the spin-spin correlation function, defined as

$$C_{cf}(r=0) = \langle (n^c_{i\uparrow} - n^c_{i\downarrow})(n^f_{i\uparrow} - n^f_{i\downarrow}) \rangle = \langle m^c_i \cdot m^f_i \rangle. \tag{7}$$

It evaluates the magnetic correlations between the c orbital and f orbital on the same site. Even though the magnetic long-range order diminishes as V increases, the magnetic correlation between the c and f orbitals increases. The minus sign indicates the anti-ferromagnetic correlations between the two orbitals on the same site. As V increases the increase of the magnitude of spin-spin correlation is a direct result of the increasing of the Kondo coupling.

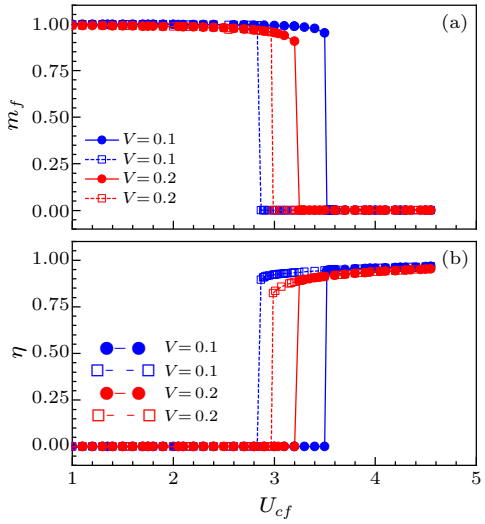

Fig. 4. The f orbital staggered magnetization m_f (a) and charge order parameter η (b) as functions of U_{cf}. Blue lines are order parameters for $V = 0.1$, and red lines are order parameters for $V = 0.2$. The solid lines are calculations starting from the AF phase, and dashed lines are calculations starting from the CO phase. The discontinuity of the lines and the hysteresis loop indicate that the phase transition is of the first order. Within the hysteresis loop is the coexistence region.

When the hybridization strength V is large, the Kondo effect dominates. However, when V has a relatively small value, the interplay of RKKY interactions and inter-orbital Coulomb repulsion plays more important role. By fixing $V = 0.1$ and $V = 0.2$, we can find the coexistence region of charge order phase and anti-ferromagnetic phase as displayed in Fig. 4. The blue lines are the corresponding order parameters of the two different order when $V = 0.1$, while the red lines are the order parameters when $V = 0.2$. Our calculations include two process, one is starting from small U_{cf} in the anti-ferromagnetic phase (solid circles in Fig. 4), the other is starting from large U_{cf} in the charge order phase (hollow squares in Fig. 4). In both the processes we use the previous result as the initial guess of the next calculation. Then we obtain the hysteresis loop just as the magnetic hysteresis loop. When $V = 0.1$ if we start from the anti-ferromagnetic phase, the magnetic phase will disappear at $U_{cf} = 3.52$, and the charge order will be present immediately. If we start from the charge order phase, the charge order will also disap-

pear and the anti-ferromagnetic phase will be present at $U_{cf} = 2.83$. Between $U_{cf} = 2.83$ and $U_{cf} = 3.52$ is the coexistence region of the two different ordered phase. The existence of the two-phase coexistence is a typical behavior of the first order transition. The discontinuities of two order parameters in Fig. 4 also indicate the phase transition is of the first order. When $V = 0.2$ the phase transition is still of the first order, the coexistence of the two phases is present too. The coexistence region is between $U_{cf} = 2.97$ and $U_{cf} = 3.25$, it becomes narrower as compared with $V = 0.1$.

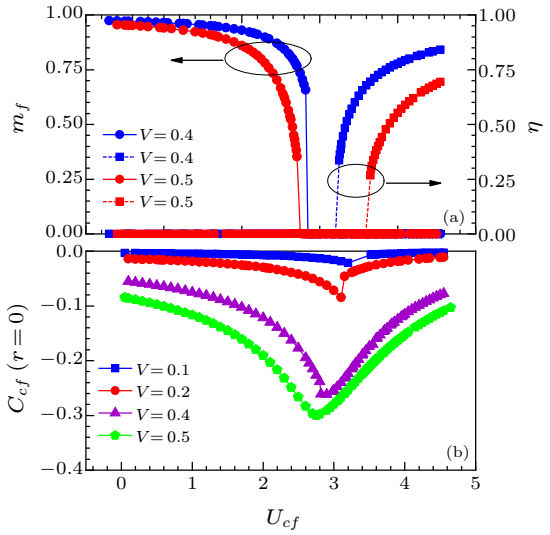

Fig. 5. (a) The order parameters, when $V = 0.4$ (blue lines) and $V = 0.5$ (red lines). The staggered magnetization of f orbital, m_f, is displayed as solid lines (circles), and the charge order parameter η is displayed as dashed lines (squares). (b) The spin-spin correlation function between c orbital and f orbital on the same site. The blue, red, purple and green lines correspond to $V = 0.1$, $V = 0.2$, $V = 0.4$ and $V = 0.5$.

The increasing V leads the coexistence region to become narrower and narrower. When V is quite close to 0.35, the coexistence region disappears as shown in Fig. 1. We also investigate how the order parameter changes when $V = 0.4$ and $V = 0.5$. The results are displayed in the upper panel of Fig. 5. The blue lines are the results when $V = 0.4$, while the red lines are the results when $V = 0.5$. As U_{cf} increases from 0, the system is in an anti-ferromagnetic phase, para-magnetic phase and charge order phase. The staggered magnetization is nonzero in the anti-ferromagnetic phase, and zero in the other two phases. The charge order parameter η is nonzero in the charge order phase, and zero in the other two phases. When $2.85 < U_{cf} < 3.20$ and $V = 0.4$, the system is in the para-magnetic phase, in which both the kinds of order parameters are zero. The region of para-magnetic phase becomes wider as V increases. When $V = 0.5$, the para-magnetic region is within $2.75 < U_{cf} < 3.59$.

Finally, the behaviors of the spin-spin correlation function $C_{cf}(r = 0)$ are shown in Fig. 5(b). The blue, red, magenta and green lines correspond to $V = 0.1$, $V = 0.2$, $V = 0.4$ and $V = 0.5$. As mentioned above, with increasing V, the magnitude of $C_{cf}(r = 0)$ also increases. This is due to the fact that the Kondo effect strengthens as V increases. Then the spin-spin correlations between onsite c and f orbitals are strengthened. Meanwhile it is interesting to see how V changes as U_{cf} varies. The magnitude of the spin-spin correlation is firstly increasing as U_{cf} increases, reaches a maximum, and then decreases. When $V = 0.4$ and $V = 0.5$, the paramagnetic phase is present, and the maximum point of the spin-spin correlation function is quite close to the critical point of the magnetic transition. In the paramagnetic phase and the CO phase, the spin-spin correlation becomes weaker and weaker since U_{cf} plays a more and more essential role, and the charge-charge correlation becomes stronger and stronger. When $V = 0.1$ and $V = 0.2$, the spin-spin correlation function displayed in Fig. 5 is calculated from a small value of U_{cf} (start from the AF phase). The maximum point of the spin-spin correlation function is located within the coexist region of the two ordered phases. The discontinuities of the blue and red lines provide another evidence of the first order transition.

We have studied the phase diagram of the EPAM on a honeycomb lattice. The interplay of the RKKY interaction, the Kondo effect and interorbital Coulomb repulsion leads to three different phases. The RKKY interaction induces the AF phase, the interorbital Coulomb repulsion induces the CO phase, and the Kondo effect kills both the long-range orders. When the Kondo effect is weak, there is one coexistence region of CO phase and AF phase. The coexistence region is present since the phase transition between the two phases is of the first order. The Kondo effect becomes stronger and stronger as V increases. Near $V = 0.35$ the coexistence region starts to disappear. In this work we only focus on the symmetric case for $E_f = -U/2$. When the system is away from the symmetric case, the valence fluctuation would play a more essential role, and we are preparing a paper about it. To describe the physics occurring in real materials, it is more important to study the system away from half filling. The honeycomb lattice studied here is bipartite. However, if tripartite lattice such as triangular lattice or Kagome lattice is studied, several more exotic phases would present. Besides the above aspects, the paramagnetic phase requires more detailed study. This is due to the fact that weakly magnetic correlation and strongly magnetic correlation lead to quite different results, not to mention what would occur when the charge correlation takes a

more important role. Moreover, the critical behaviors of the entangled spectra is worth studying, as it would provide significant information on the quantum phase transitions.[31]

References

[1] Lawrence J M, Riseborough P S and Parks R D 1981 *Rep. Prog. Phys.* **44** 1
[2] Watanabe S, Tsuruta A, Miyake K and Flouquet J 2009 *J. Phys. Soc. Jpn.* **78** 104706
[3] Miyake K and Watanabe S 2017 *Philos. Mag.* **97** 3495
[4] Nakatsuji S, Kuga K, Machida Y, Tayama T, Sakakibara T, Karaki Y, Ishimoto H, Yonezawa S, Maeno Y, Pearson E, Lonzarich G G, Balicas L, Lee H and Fisk Z 2008 *Nat. Phys.* **4** 603
[5] Okawa M, Matsunami M, Ishizaka K, Eguchi R, Taguchi M, Chainani A, Takata Y, Yabashi M, Tamasaku K, Nishino Y, Ishikawa T, Kuga K, Horie N, Nakatsuji S and Shin S 2010 *Phys. Rev. Lett.* **104** 247201
[6] Watanabe S and Miyake K 2010 *Phys. Rev. Lett.* **105** 186403
[7] Utsumi Y, Sato H, Kurihara H, Maso H, Hiraoka K, Kojima K, Tobimatsu K, Ohkoch T, Fujimori S I, Takeda Y, Saitoh Y, Mimura K, Ueda S, Yamashita Y, Yoshikawa H, Kobayashi K, Oguchi T, Shimada K, Namatame H and Taniguchi M 2011 *Phys. Rev. B* **84** 115143
[8] Gegenwart P, Custers J, Tokiwa Y, Geibel C and Steglich F 2005 *Phys. Rev. Lett.* **94** 076402
[9] Wada S, Yamamoto A, Ishida K and Sarrao J L 2008 *J. Phys.: Condens. Matter* **20** 175201
[10] Lashley J C, Lawson A C, Cooley J C, Mihaila B, Opeil C P, Pham L, Hults W L, Smith J L, Schmiedeshoff G M, Drymiotis F R, Chapline G, Basu S and Riseborough P S 2006 *Phys. Rev. Lett.* **97** 235701
[11] Yuan H Q 2003 *Science* **302** 2104
[12] Yamaoka H, Ikeda Y, Jarrige I, Tsujii N, Zekko Y, Yamamoto Y, Mizuki J, Lin J F, Hiraoka N, Ishii H, Tsuei K D, Kobayashi T C, Honda F and Onuki Y 2014 *Phys. Rev. Lett.* **113** 086403
[13] Phan V N 2020 *Phys. Rev. B* **101** 245120
[14] Chatterjee S, Ruf J P, Wei H I, Finkelstein K D, Schlom D G and Shen K M 2017 *Nat. Commun.* **8** 852
[15] Danzenbacher S, Vyalikh D V, Kucherenko Y, Kade A, Laubschat C, Caroca-Canales N, Krellner C, Geibel C, Fedorov A V, Dessau D S, Follath R, Eberhardt W and Molodtsov S L 2009 *Phys. Rev. Lett.* **102** 026403
[16] Dubi Y B A V 2011 *Phys. Rev. Lett.* **106** 086401
[17] Watanabe S, Imada M and Miyake K 2006 *J. Phys. Soc. Jpn.* **75** 043710
[18] Saiga Y, Sugibayashi T and Hirashima D S 2008 *J. Phys. Soc. Jpn.* **77** 114710
[19] Onishi Y and Miyake K 2000 *J. Phys. Soc. Jpn.* **69** 3955
[20] Yoshida T, Ohashi T and Kawakami N 2011 *J. Phys. Soc. Jpn.* **80** 064710
[21] Yoshida T and Kawakami N 2012 *Phys. Rev. B* **85** 235148
[22] Takemura S, Takemori N and Koga A 2015 *Phys. Rev. B* **91** 165114
[23] Hagymasi I, Itai K and Solyom J 2013 *Phys. Rev. B* **87** 125146
[24] Hagymasi I, Solyom J and Legeza O 2014 *Phys. Rev. B* **90** 125137
[25] Phan V N, Mai A and Becker K W 2010 *Phys. Rev. B* **82** 045101
[26] Knizia G and Chan G K L 2012 *Phys. Rev. Lett.* **109** 186404
[27] Yang J W, Wang Q Y, Ma T X and Chen Q N 2019 *Phys. Rev. B* **99** 245136
[28] Yang J W and Chen Q N 2018 *Chin. Phys. B* **27** 37101
[29] Sharma S and Chan G K L 2012 *J. Chem. Phys.* **136** 124121
[30] Chen Q N, Booth G H, Sharma S, Knizia G and Chan G K L 2014 *Phys. Rev. B* **89** 165134
[31] Tang Q C and Zhu W 2020 *Chin. Phys. Lett.* **37** 010301